Tissue-Specific Patterns of Lignification Are Disturbed in the *brown midrib2* Mutant of Maize (*Zea mays* L.)

Wilfred Vermerris*,† and Jaap J. Boon‡

Department of Botany and Plant Pathology, 1155 Lilly Hall, Purdue University, West Lafayette, Indiana 47907, and FOM Institute for Atomic and Molecular Physics, Kruislaan 407, 1098 SJ Amsterdam, The Netherlands

Despite recent progress, several aspects of lignin biosynthesis, including variation in lignin composition between species and between tissues within a given species, are still poorly understood. The analysis of mutants affected in cell wall biosynthesis may help increase the understanding of these processes. We have analyzed the maize *brown midrib2* (*bm2*) mutant, one of the four *bm* mutants of maize, using pyrolysis−mass spectrometry (Py−MS) and pyrolysis−gas chromatography−mass spectrometry (Py−GC−MS). Vascular tissues from the leaf blade and leaf sheath from different parts of the plant were investigated and compared to the corresponding samples from a wild-type plant of the same genetic background (inbred line A619). Multivariate analysis revealed that the *bm2* mutant had reduced amounts of di- and trimeric lignin derivatives, notably species with *m*/*z* 272 and *m*/*z* 330, and that the ratio of guaiacyl residues to polysaccharides was reduced in the *bm2* mutant. In addition, differences in cell wall composition between different parts of the plant (blade versus sheath, young versus old tissue) were much less pronounced in the *bm2* mutant. These changes suggest that the functional *Bm2* gene is important for the establishment of tissue-specific cell wall composition.

Keywords: *Bm2; brown midrib; lignin; maize; pyrolysis−mass spectrometry; Zea mays*

INTRODUCTION

The *brown midrib2* (*bm2*) mutant of maize (*Zea mays* L.) displays a reddish-brown coloration of the vascular tissue in the leaf and stem, which becomes first visible at the four-leaf stage (*1*). The *bm2* mutant is one of the four *brown midrib* mutants of maize. These mutants have a reduced lignin content and altered lignin composition (*2*).

Although many steps in the lignin biosynthetic pathway have been elucidated (reviewed by Boudet (*3*) and Whetten et al. (*4*)), there are still several aspects of lignin biosynthesis and its regulation that are poorly understood. This includes the basis for differences in lignin composition between species (gymnosperms versus angiosperms) and within species. An example of the latter case is the lignin composition in *Arabidopsis*. Lignin in the tracheary elements of vascular bundles was shown to be composed mostly of guaiacyl units, whereas lignin in the sclerenchyma of the stem also contains syringyl units (*5*). Similar observations have been made in maize (*6* and *7*). The analysis of naturally occurring mutants such as the *brown midrib* mutants of maize and sorghum, or the use of (anti)sense strategies to down-regulate specific metabolic steps, can help to improve our understanding of how specific genes influence lignin composition. Thus, the maize *bm1* mutation was shown to affect the enzyme cinnamyl alcohol dehydrogenase (CAD), resulting in lignin with increased amounts of coniferaldehyde (*8*). The lignin of the maize *bm3* mutant was shown to contain 5-hydroxyguaiacyl residues and contained fewer syringyl residues (*9*) because of a mutation in the gene encoding the enzyme caffeic acid *O*-methyl transferase (*10*). In addition, their reduced lignin content and altered cell wall properties have made the *bm* mutants interesting from an agronomic perspective, because of the potential for improved forage quality (*11*). The function of the *Bm2* gene has not yet been elucidated, although the lignin of the *bm2* mutant was recently analyzed using both thioacidolysis and nitrobenzene oxidation (*12*). These experiments indicated that the lignin of the *bm2* mutant had a reduced content of guaiacyl residues and an increase in syringyl residues. The increase in syringyl units was not consistent between the two methods: thioacidolysis indicated a 40% increase, but nitrobenzene oxidation indicated a 15% increase. This discrepancy was attributed to the different interunit linkages that are disrupted by the two methods; the increase in syringyl subunits was supposedly mostly in noncondensed (*β*-*O*-4 linked) lignin.

A potential complicating factor with the analysis by Chabbert et al. (*12*) is the fact that the genetic background was not the same for the *bm2* mutant and their wild-type control. It has been demonstrated that the genetic background can have a significant effect on lignin content (*13*) and cell wall composition in maize (*14*), and differences in genetic background can also affect growth and development, and therefore complicate sampling.

In this study we have compared a *bm2* mutant with a wild-type plant of the same genetic background. Differences in lignin composition can therefore be attributed more rigorously to the single mutant gene.

* Author for correspondence. Telephone: +765-494-6140. Fax: +765-494-0363. E-mail: vermerris@purdue.edu.
† Purdue University.
‡ FOM Institute for Atomic and Molecular Physics.

10.1021/jf000740r CCC: $20.00
Published on Web 12/15/2000

Most analyses of the effects of *bm* mutations on lignin have been performed on mature plants (silage stage) (see for example *12* and *15*). This makes sense when the emphasis is on changes in cell wall composition that may affect the nutritional value of the plant. However, as the plant matures, the cell walls get enriched with syringyl residues and they accumulate substantial amounts of *p*-coumaric acid (*14*−*16*). To prevent masking of subtle differences by these developmental effects, we have harvested the plant material before maturity, i.e., when the tassel was just emerging. For the analysis of the cell wall material we have used pyrolysis−mass spectrometry (Py−MS), and pyrolysis−gas chromatography−mass spectrometry (Py−GC−MS). These techniques have been shown to be informative in the analysis of ligno-cellulosic material (*14*, *17*−*19*). Both techniques were also used in combination with the methylating agent tetra methylammonium hydroxide (TMAH). This provides additional information on the cell wall composition, in particular on lignin subunits, *p*-coumaric acid, and ferulic acid (*20*). A major advantage of analytical pyrolysis over most other chemical analyses is that it requires only small amounts of sample. This allowed us to identify tissue-specific changes as a result of the *bm2* mutation.

MATERIALS AND METHODS

Plant Material. The generation of the *bm2* near-isogenic line (NIL) was described by Vermerris and McIntyre (*21*). The *bm2* NIL and inbred A619 plants were grown in the field in Clayton, NC. Two plants of each genotype were harvested when the tassel was just emerging (13 leaf stage). The midrib of leaves 6 and 7, and the leaf sheaths covering internodes 6 and 10 were removed. The vascular tissue was dissected from the midribs and from the top and bottom third of the leaf sheaths. These vascular tissues were chosen because they could be dissected easily and cleanly, and wild-type and *bm2* samples displayed a clear difference in color. Pieces of vascular tissue of approximately 2 mm in length were extracted in water (2 × 30 min) to remove water-soluble compounds, and in acetone (2 × 30 min) to remove unbound phenolic compounds.

Pyrolysis−MS. Py−MS analyses (in direct temperature resolved MS mode) were performed according to Pillonel et al. (*18*), and Py−MS analyses of tetramethylammonium hydroxide (TMAH)-treated samples were performed according to Mulder et al. (*20*). Between 5 and 10 μg of an aqueous cell wall suspension was applied to the wire and dried in vacuo. An aliquot of 5 μL of TMAH (2.5% solution in water) was added for direct-probe thermally assisted trans-methylation studies. Pyrolysis was carried out using an insertion probe equipped with a resistively heated loop-shaped Pt/Rh (9/1) filament (100 μm diameter) inside the ion source of a JEOL SX-102A double-focusing mass spectrometer (reversed geometry B/E). Ionization was performed under electron ionization (EI) or ammonia chemical ionization conditions (CI). The mass spectrometer was operated at 10 kV. The mass range was scanned from *m*/*z* 20−1000 (EI) or *m*/*z* 60−1000 (CI) with a cycle time of 1 s. Data were acquired and processed using the JEOL MP7000 data system. Data were exported to a high-speed PC for further data processing by multivariate analysis.

Pyrolysis MS−MS. A custom-built collision cell behind the magnet just before the electron sector allowed the performance of mass-analyzed ion kinetic energy spectroscopy (MIKES) studies of selected ions. The analysis was performed on *m*/*z* 330. The analysis had to be performed in a multichannel averaging mode of the data acquisition for reasons of sensitivity. Helium was used as the collision gas.

Multivariate Analysis. The set of mass spectra contains a large amount of information. A multivariate analysis was performed in order to identify sets of mass peaks whose intensity was significantly different between the various samples. We performed a discriminant analysis (double-stage principal component analysis) on the data. The principle of double-stage principal component analysis of mass spectra has been described by Hoogerbrugge et al. (*22*). The FOMpyroMAP and Chemometriks programs were used for this analysis according to the description in Klap et al. (*23*). The goal of this analysis is to explain the variance−covariance structure of the data set through linear combinations of the original variables (*24*). Briefly, the spectra of individual samples are represented as points in a multidimensional mass-vector space with the mass numbers as coordinates. The position of a particular sample in this multidimensional space is determined by the relative distribution of mass intensities in the spectrum of this sample. Similar spectra cluster together in this multidimensional space. A weighted-average spectrum can be defined, serving as a reference for individual spectra. The differences in the set of samples can be expressed as deviations from the weighted-average spectrum, and orthogonal axes through this average are chosen in such a way that the between-sample variance is maximal. The positions of the individual samples can then be defined by their projections (scores) on the resulting axes (principal components). In discriminant analysis, the principal component spectra are reanalyzed in the same way, but this time information is provided on the existence of replicate analyses in the data set. The end result of this part of the analysis is the minimization of the within-sample variance. The discriminant functions are ranked on the basis of characteristic variance, i.e., the amount of total variance explained, and the minimization of the within-sample variance. The geometric distance in multivariate space of the different samples can be represented graphically in score-plots. The discriminant functions can also be translated into discriminant function spectra which show the mass peaks contributing to the differences between samples and are therefore easier to interpret than the original spectra. Note that the sample size in double-stage principal component analysis is a function of the number of mass peaks that is considered in the analysis, which can be up to 700 per sample.

Py−GC−MS. Selected native or TMAH-treated samples were analyzed by Py−GC−MS as described in Mulder et al. (*20*) using a FOM-4LX Curie point pyrolyzer. Homogenized sample suspension and reagent solution were applied to ferromagnetic probes (Curie point of 510 °C) which were inserted into a glass liner. The pyrolysis of trans-methylated products was analyzed on a Carlo Erba/Fisons HRGC 8565 gas chromatograph coupled to a JEOL DX-303 double-focusing mass spectrometer. The capillary column (25 m, 320-μm i.d., fused silica coated with SGE BPX-5) was inserted directly in the ion source using a custom-built heatable interface set at 300 °C. The GC was programmed from 50 to 350 °C with a temperature ramp of 4 °C/min. Helium was used as carrier gas.

RESULTS

A pyrogram of the vascular tissue from wild-type and *bm2* midrib (leaf 7) is shown in Figure 1. When these pyrograms and those representing the other tissue samples are compared, a number of differences can be observed. The fragments with an *m*/*z* value less than 100 amu, as well as the fragments of 114, 126, and 144 amu, originate from polysaccharides. The samples from the *bm2* mutant tend to have more of these fragments than the wild-type samples. The fragments with *m*/*z* values larger than 100 amu are mostly $M^{\bullet+}$ ions that are indicative of specific compounds, primarily lignin and hydroxycinnamic acids. The *bm2* mutant has fewer fragments derived from guaiacyl subunits [for example coniferyl alcohol (*m*/*z* 180 $[M]^+$, 137 $[M\text{-}43]^+$, 124) and coniferyl aldehyde (*m*/*z* 178 $[M]^+$, 135 $[M\text{-}43]^+$)], whereas the fragments derived from syringyl subunits do not seem to be affected significantly [(sinapyl alcohol (*m*/*z*

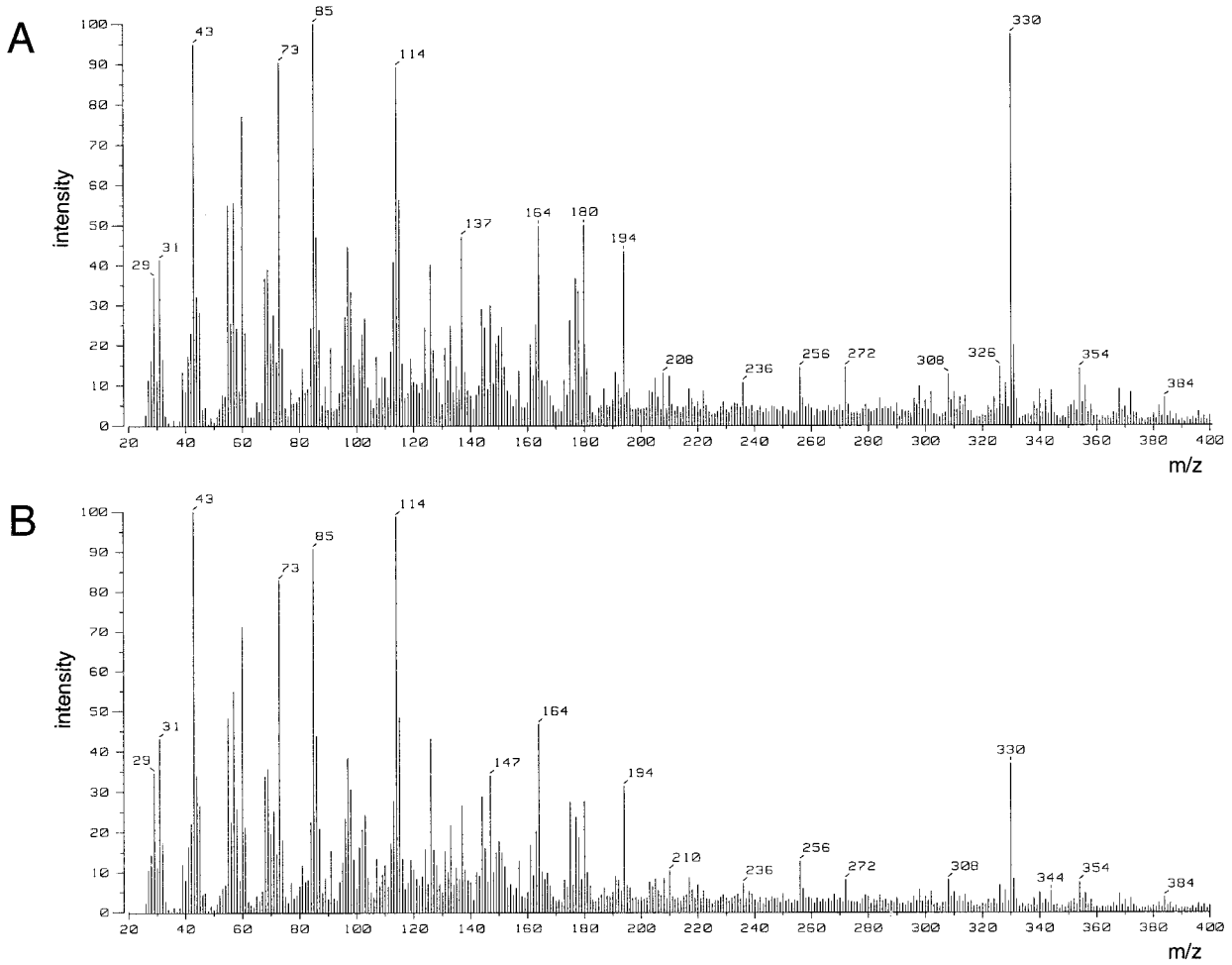

Figure 1. Pyrograms of dissected vascular tissue from the midrib of leaf 7: (A) wild type; (B) *bm2*. The *m/z* ratio is plotted along the horizontal axis, the intensity is plotted along the vertical axis.

210 $[M]^+$, 167 $[M-43]^+$, and 154) and sinapyl aldehyde (*m/z* 208, 165 $[M-43]^+$)]. The fragments with *m/z* values higher than about 250 amu are mostly dimeric and trimeric structures derived from lignin. The compounds with *m/z* values of 272 (3,3′-dimethoxy-4,4′-dihydroxystilbene) and 330 (compound unknown) amu are drastically reduced in the *bm2* mutant; many other, less abundant, high molecular weight fragments also show a reduction.

To ascertain whether the *bm2* mutation affects the amount of cell wall bound *p*-coumaric and ferulic acid we performed Py−GC−MS and Py−MS with TMAH-treated samples. Figure 2 shows the gas chromatogram in which the peaks corresponding to *p*-coumaric acid (after methylation *m/z* 192 and 161 $[M-31]^+$), ferulic acid (after methylation *m/z* 222 and 191 $[M-31]^+$), and *m/z* 330 (observed after methylation at *m/z* 358) have been selectively displayed. No major differences were observed between the *bm2* mutant and the wild type with respect to *p*-coumaric acid and ferulic acid, but it is again clear how the *bm2* mutation causes a major reduction in the dimeric structure of 330 amu. The exact structure of the dimeric compound of 330 amu is unknown at this point, but the ion has been observed in MS data of lignin and plant tissues from several grasses (Boon, unpublished data). MIKES studies of *m/z* 330 provided evidence that fragmentation is limited to formation of several diagnostic fragments at *m/z* 153 and 178, indicative of methoxylated phenolic structural elements and fragments derived from the intact, presumably highly stabilized, aromatic structure (Figure 3). The *m/z* 153 could be due to an alfa-cleavage leaving a dimethoxylated phenolic ring structure. The even ion *m/z* 178 must be a result of a rearrangement and points to a H-shift to the residual ion formed by loss of the syringyl unit from the parent (*m/z* 330). There is no loss of water from *m/z* 330 which excludes the presence of exocyclic hydroxyl groups. The compound with the MW of 330 does not elute from the GC, but its methylated derivative does (see Figure 2). This behavior is interpreted as indicative of a structure with two hydroxyl moieties that can be methylated, resulting in a compound of 358 amu after TMAH treatment. The reference compound 5-5′diacetovanillone (kindly provided by Dr. J. Ralph (U.S. Dairy Forage Research Center, Madison, WI) was considered as a candidate for *m/z* 330 because of the existence of a C−C linkage between the two phenolic rings and because of its highly conjugated structure. Comparative studies under similar analytical conditions with 5-5′diacetovanillone, however, demonstrated that this compound did not match the Py−TMAH−GC−MS or the MIKES data of *m/z* 330 (data not shown). An additional 17 isomers on the basis of potential coumarone and stilbene structures have been considered. Unfortunately, the reference compounds are not available, and on paper none of these structures fit the data without considerable bias. Attempts to identify *m/z* 330 continue.

A double-stage principal component analysis was performed to identify chemical differences between the

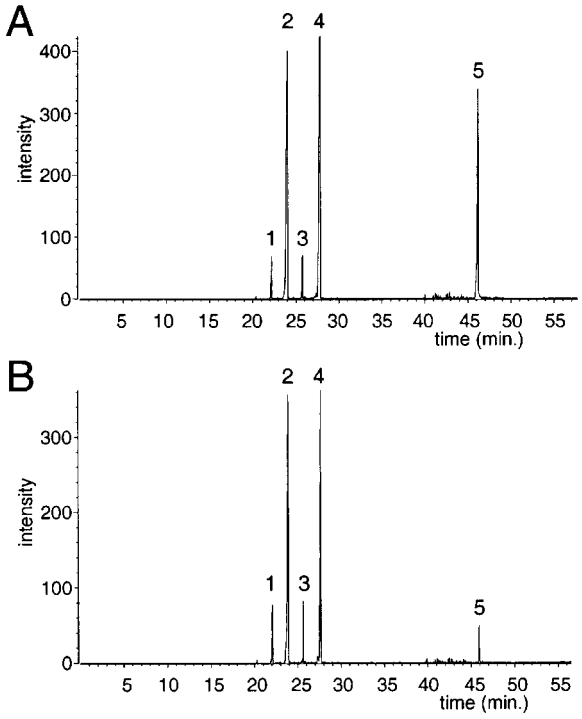

Figure 2. Py−TMAH−GC−MS data of dissected vascular tissue from the sheath surrounding the top of internode 6 of (A) wild type and (B) *bm2*. Transmethylated compounds have been selected from the complete chromatogram: (1) *cis-p*-coumaric acid (*m*/*z* 192); (2) *trans-p*-coumaric acic (*m*/*z* 192); (3) *cis*-ferulic acid (*m*/*z* 222); (4) *trans*-ferulic acid (*m*/*z* 222); and (5) the unknown compound *m*/*z* 330 (358 after transmethylation).

various samples. Figure 4 shows the reconstructed mass spectra of the first two discriminant functions, DF1 and DF2. DF1 explains 74% of the total variance, and is based on fragments derived from polysaccharides ($DF1^+$) and from guaiacyl residues, including several dimeric structures ($DF1^-$) (Figure 4A, B). DF2 explains 16% of the total variance and also makes a distinction based on polysaccharides and guaiacyl residues (Figure 4C, D). The unknown compound *m*/*z* 330 is a major contributor in both DF1 and DF2. After calculating the corresponding discriminant function scores, the wild-type and *bm2* samples are clearly separated along the DF1-axis in the score-plot (Figure 5). The positive scores for the *bm2* samples reflect that the pyrolysate of these samples contains more fragments derived from polysaccharides, whereas the pyrolysate of the wild-type samples (negative function scores) contains more fragments derived from guaiacyl residues. In addition, *m*/*z* 330 and many other high-molecular-weight fragments representing dimers and trimers derived from lignin are more abundant in the wild-type samples than in the *bm2* samples. The score-plot also shows how the different tissues of the wild-type plant are clearly separated along the DF2 axis (Figure 5). This separation is consistent with the developmental age of the samples. The midrib samples, which are the most mature, contain more guaiacyl residues than the vascular tissue from the top and bottom of the sheath. The bottom of the sheath, where lignification occurs last, is relatively rich in polysaccharides (positive function scores). In contrast to the clear separation of tissues observed for the wild-

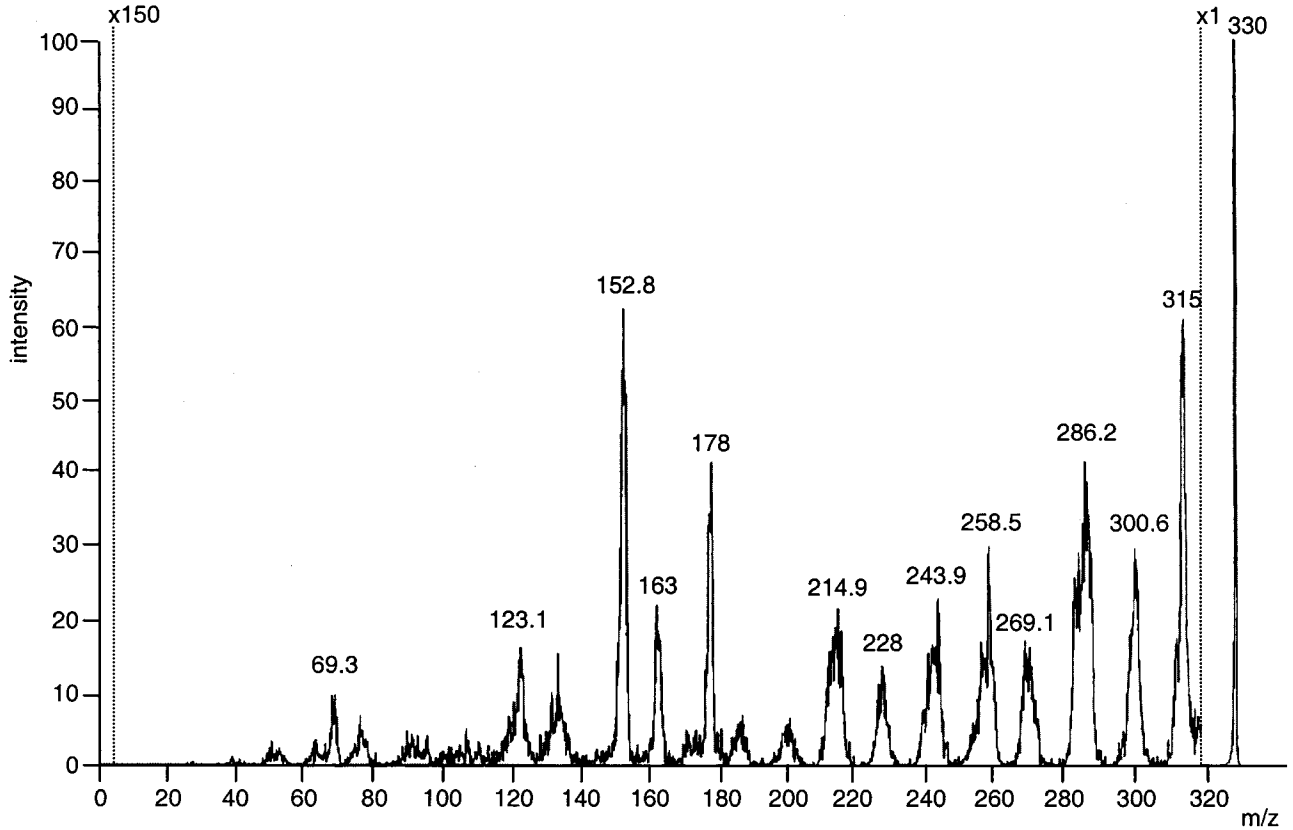

Figure 3. Py−MS−MS analysis (MIKES) of maize compound *m*/*z* 330. The intensity is plotted along the vertical axis, the *m*/*z* ratio is plotted along the horizontal axis. The dotted lines indicate the magnification of the peaks to the right of the lines; the magnification factor is indicated above the line.

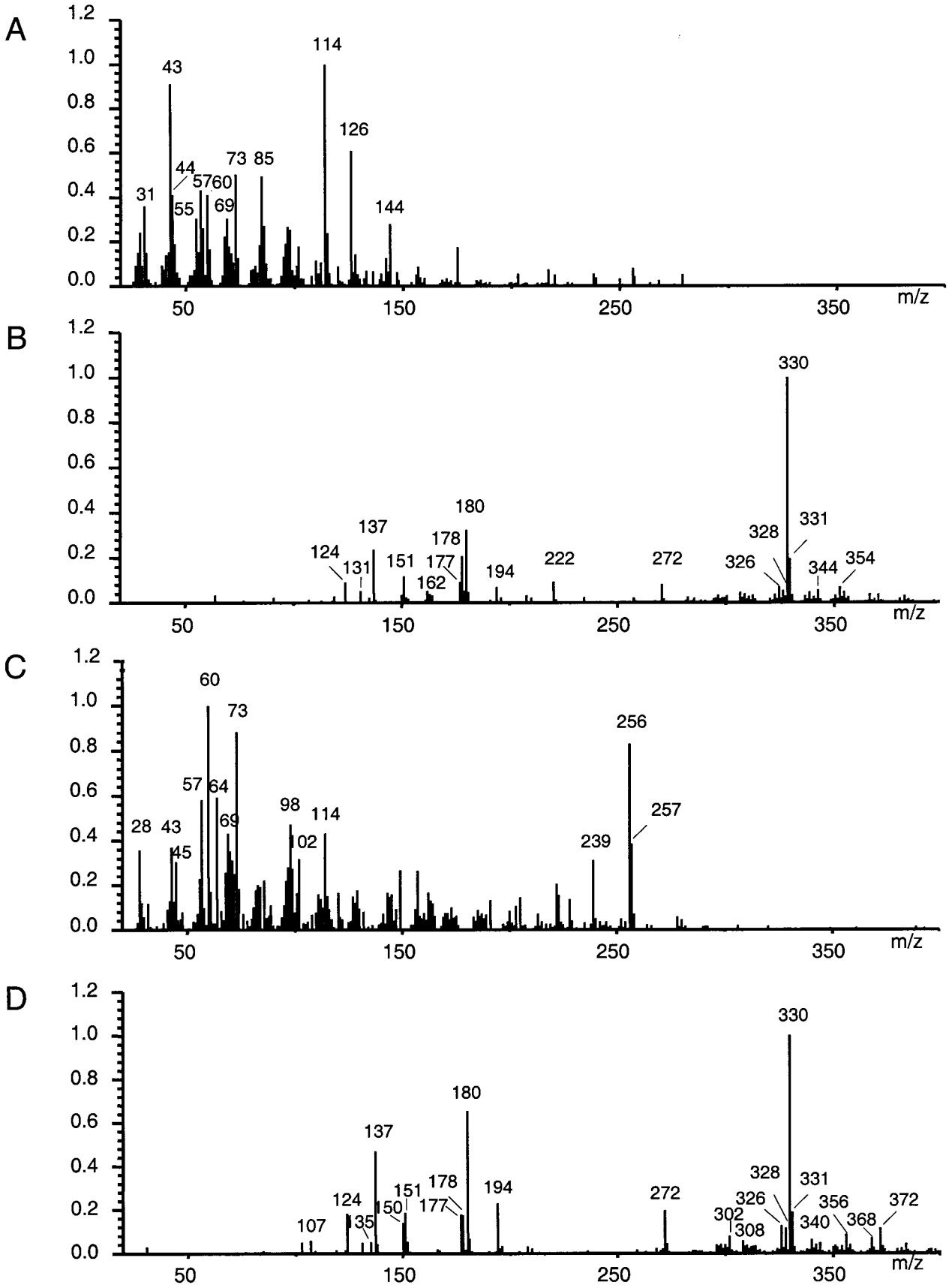

Figure 4. Discriminant function spectra (A) $DF1^+$, (B) $DF1^-$, (C) $DF2^+$, and (D) $DF2^-$. The *m/z* ratio is plotted along the horizontal axis. The *y*-axis indicates the ratio between the intensity of a given peak and the intensity of the highest mass peak present.

type plant, the different tissues from the *bm2* mutant are not separated clearly along the DF2 axis. Instead, they overlap extensively and cluster near the center of the DF2 axis, indicative of little variation. This indicates that the tissue-specific lignification is disturbed in the *bm2* mutant. This disturbance is associated with a reduction in guaiacyl residues in general, and *m/z* 330 in particular.

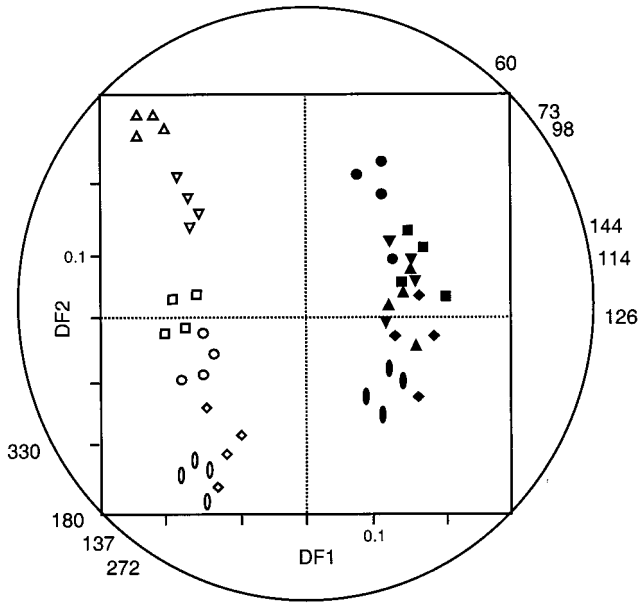

Figure 5. Score-plot for the Py−MS spectra of vascular tissue from wild-type and *bm2* plants. Four tissue samples from each of the following tissues were analyzed: sheath from the bottom of internode 6 (△), the bottom of internode 10 (▽), the top of internode 6 (□), and the top of internode 10 (○), and midrib from leaf 6 (◇) and 7 (elongated oval). The open symbols represent the wild-type samples and the closed symbols represent the *bm2* samples. DF1 separates the *bm2* samples (positive discriminant function scores) from the wild-type samples (negative discriminant function scores), indicative of high and low ratios of polysaccharides to guaiacyl residues, respectively. DF2 identifies tissue-specific differences in cell wall composition in the wild-type plant, but these differences are absent in the *bm2* mutant. The differences in the wild type are based on the ratio of polysaccharides to guaiacyl residues. This ratio is lower when the discriminant function score for DF2 is negative. The numbers placed outside the circle indicate a selection of *m*/*z* values of fragments contributing to the discriminant functions. Vectors originating in the center of the circle and pointing to the position of a specific *m*/*z* value can be projected on the DF1 and DF2 axes to indicate their relative contributions to those discriminant functions. For example, *m*/*z* 330 contributes to both $DF1^-$ and $DF2^-$, whereas *m*/*z* 126 contributes to $DF1^+$, but not to DF2 (see also Figure 4).

DISCUSSION

In contrast to the *bm1* and *bm3* mutations in maize (*8* and *9*) and the *bmr6* mutation in sorghum (*18* and *25*), the *bm2* mutation does not appear to result in the accumulation of intermediates from the lignin biosynthetic pathway. Instead, the changes are subtle and point toward mainly structural changes, as evidenced by the reduction in *m*/*z* 330 and other di- and trimeric structures derived from lignin, and a reduction in guaiacyl residues without an effect on syringyl residues. The maize internode develops basipetally, resulting in a developmental gradient with the oldest tissue at the top and the youngest tissue at the bottom of the internode. Because the older tissue is more heavily lignified, a lignin gradient is formed along the internode (*26*). The data presented here indicate that this lignin gradient is disrupted in the *bm2* mutant.

The reduction in guaiacyl subunits agrees with the report by Chabbert et al. (*12*), but the increase in syringyl subunits that they reported was not confirmed in this analysis. The lack of agreement on the syringyl subunits could be the result of differences in sampling. In maize, syringyl subunits are deposited late in plant development (*14* and *16*). Chabbert et al. (*12*) used plants that were at the silage stage, whereas the plants that we analyzed were harvested when the tassel was just emerging. It is therefore possible that the effect of the *bm2* mutation on syringyl subunits is only detectable late in plant development. It is also possible that the effect on syringyl subunits is dependent on the type of tissue. Chabbert et al. (*12*) analyzed cell wall fractions derived from the stem, but we analyzed the vascular tissue from the leaf blade and sheath. Alternatively, the difference in syringyl subunits reported by Chabbert et al. (*12*) may have been (partly) due to genetic variation, because they did not use near-isogenic lines. It is noteworthy, however, that even though Chabbert et al. (*12*) did not specifically mention this, their data (their Table 2) provide independent support for our finding that the gradient of guaiacyl residues across the internode is disrupted in the *bm2* mutant.

Traditionally, the analysis of mutants provides a mechanism to uncover the normal function of the gene of interest. Therefore, based on the phenotype of the *bm2* mutant described here, we can attempt to unravel the function of the *Bm2* gene in lignification. The *Bm2* gene could encode an enzyme involved in the biosynthesis of coniferyl alcohol. This is, however, unlikely for two reasons. First, metabolic blocks in the lignin biosynthetic pathway typically result in the accumulation of intermediates or unusual cell wall components, both in mutants (*8*, *9*, *27*), and in transgenic plants in which the activity of lignin biosynthetic enzymes has been reduced via (anti)sense technology (*28* and *29*). We have no evidence for the accumulation of such intermediates in the *bm2* mutant. Second, recent reports have indicated that syringyl residues in *Arabidopsis* and *Magnolia kobus* are synthesized from coniferyl alcohol or its precursors (*30*−*32*). Assuming a similar mechanism for maize, a block in the biosynthesis of coniferyl alcohol would be expected to lead to a reduction in syringyl subunits. The *bm2* mutant, however, appears to have normal levels of syringyl residues.

A more likely explanation for the reduction in guaiacyl residues is a disturbance in the transport of monolignols. In considering a disturbance in the transport of monolignols to explain the changes in the *bm2* mutant, we need to assume a specific effect on coniferyl alcohol (or its glucoside), because syringyl subunits are apparently not affected. To examine this hypothesis it will be necessary to study tissues actively undergoing lignification, possibly with the help of radiolabeled substrates.

A third explanation for a reduction in guaiacyl residues is that the *bm2* mutation affects the polymerization of guaiacyl residues. Whether the process of lignin polymerization is random or mediated by specific proteins is currently an area of debate. The reduction in *m*/*z* 330 in the *bm2* samples, and its correlation with lack of tissue-specificity argues for some degree of organization. In addition to the model proposed by Gang et al. (*33*) regarding the formation of stereospecific linkages between monolignols, it is possible that proteins in the cell wall have a function in cross-linking lignin, possibly via tyrosine residues (*7*, *34*, *35*). The lack of such proteins, or a disturbance in the coordination of their deposition, may result in changes in cell wall composition similar to what we described here for the *bm2* mutant.

Finally, the *Bm2* gene may be a regulator involved in the spatio-temporal coordination of lignin deposition.

A disturbance in this process would result in lignification at the wrong developmental time or in the wrong location (at the cell or tissue level). Although there have been various reports on the involvement of transcription factors in the regulation of lignin biosynthesis (*36* and *37*), at this point a clear understanding of how the expression of each lignin biosynthetic gene is regulated and coordinated is lacking. This makes it difficult to ascertain whether the *bm2* phenotype is in accordance with the phenotype of a plant in which the regulation of lignin biosynthesis is disturbed.

The identity of *m*/*z* 330 may provide additional information about the function of the *Bm2* gene. The reference compound 5-5′diacetovanillone was the most plausible candidate, but this compound was excluded on the basis of the MIKES analysis. Isolation of *m*/*z* 330 by preparative Py−GC or Py−HPLC followed by NMR may help in the identification of the structure. The question remains whether the reduction in guaiacyl residues and *m*/*z* 330 is the cause or the consequence of a lack of tissue-specificity. It is difficult to investigate this, because the intermediates in the lignin biosynthetic pathway cannot be assayed easily. Hence, a reduction in the end product could be due to a reduced flux through the pathway or a reduced incorporation. Further characterization of the *bm2* mutant is likely to contribute to our understanding of lignin polymerization and tissue-specific variation in lignin composition, two processes that are not yet fully understood. Cloning of the *Bm2* gene is in progress and is expected to provide additional clues.

ACKNOWLEDGMENT

Ronald Sederoff, Paul Sisco, and Ross Whetten are acknowledged for helpful discussions. We thank William G. Brown, Jr. for excellent assistance in the field, and John Ralph and Jane Marita (U.S. Dairy Forage Research Center, Madison, WI) for providing the 5-5′diacetovanillone. Jos Pureveen, Jerre van der Horst, and Gert Eijkel are acknowledged for their technical assistance with the MS and multivariate analysis work.

LITERATURE CITED

(1) Burnham, C. R.; Brink, R. A. Linkage relations of a second *brown midrib* gene (*bm2*) in maize. *J. Am. Soc. Agron.* **1932**, *24*, 960−963

(2) Kuc, J.; Nelson, O. E.; Flanagan, P. Degradation of abnormal lignins in the brown-midrib mutants and double mutants of maize. *Phytochemistry* **1968**, *7*, 1435−1436.

(3) Boudet, A.-M. A new view of lignification. *Trends Plant Sci.* **1998**, *3*, 67−71.

(4) Whetten, R. W.; MacKay, J. J.; Sederoff, R. R. Recent advances in understanding lignin biosynthesis. *Annu. Rev. Plant Physiol. Plant Mol. Biol.* **1998**, *49*, 585−609.

(5) Chapple, C. C. S.; Vogt, T.; Ellis, B. E.; Sommerville, C. R. An Arabidopsis mutant defective in the general phenylpropanoid pathway. *Plant Cell* **1992**, *4*, 1413−1424.

(6) Joseleau, J.-P.; Ruel, K. Study of lignification by noninvasive techniques in growing maize internodes. *Plant Phys.* **1997**, *114*, 1123−1133.

(7) Müsel, G.; Schindler, T.; Bergfeld, R.; Ruel, K.; Jacquet, G.; Lapierre, C.; Speth, V.; Schopfer, P. Structure and distribution of lignin in primary and secondary cell walls of maize coleoptiles analyzed by chemical and immunological probes. *Planta* **1997**, *201*, 146−159.

(8) Halpin, C.; Holt, K.; Chojecki, J.; Oliver, D.; Chabbert, B.; Monties, B.; Edwards, K.; Barakate, A.; Foxon, G. A. *Brown-midrib* maize (*bm1*) − a mutation affecting the cinnamyl alcohol dehydrogenase gene. *Plant J.* **1998**, *14*, 545−553.

(9) Lapierre, C. Application of new methods for the investigation of lignin structure. In *Forage Cell Wall Structure and Digestibility*; Jung, H. G., Buxton, D. R., Hatfield, R. D., Ralph, J., Eds.; American Society of Agronomy (ASA-CSSA-SSSA): Madison, WI, 1993; pp 133−166.

(10) Vignols, F.; Rigau, J.; Torres, M. A.; Capellades, M.; Puigdomenech, P. The *brown-midrib3* (*bm3*) mutation in maize occurs in the gene encoding caffeic acid *O*-methyl transferase. *Plant Cell* **1995**, *7*, 407−416.

(11) Cherney, J. H.; Cherney, D. J. R.; Akin, D. E.; Axtell, J. D. Potential of brown-midrib, low-lignin mutants for improving forage quality. *Adv. Agron.* **1991**, *46*, 157−198.

(12) Chabbert, B.; Tollier, M. T.; Monties, B.; Barrière, Y.; Argillier, O. Biological variability in lignification of maize: expression of the brown midrib bm2 mutation. *J. Sci. Food Agric.* **1994**, *64*, 455−460.

(13) Lundvall, J. P.; Buxton, D. R.; Hallauer, A. R.; George, J. R. Forage quality variation among maize inbreds: in vitro digestibility and cell-wall components. *Crop Sci.* **1994**, *34*, 1672−1678.

(14) Mulder, M. M.; Dolstra, O.; Boon, J. J. Pyrolysis mass spectrometry as a scanning tool for plant breeders: a study of two public inbred lines of *Zea mays*. In *Production and Utilization of Lignocellulosics*; Galletti, G. C., Ed.; Elsevier Applied Science: London, 1991; pp 291−307.

(15) Provan, G. J.; Scobbie, L.; Chesson, A. Characterisation of lignin from CAD and OMT deficient *Bm* mutants of maize. *J. Sci. Food Agric.* **1997**, *73*, 133−142.

(16) Terashima, N.; Fukushima, K.; He, L.-F.; Takabe, K. Comprehensive model of the lignified plant cell wall. In *Forage Cell Wall Structure and Digestibility*; Jung, H. G., Buxton, D. R., Hatfield, R. D., Ralph, J., Eds; American Society of Agronomy (ASA-CSSA-SSSA): Madison, WI, 1993; pp 247−270.

(17) Boon, J. J. An introduction to pyrolysis mass spectrometry of lignocellulosic material: case studies of barley straw, corn stem and *Agropyron*. In *Physico-Chemical Characterisation of Plant Residues for Industrial and Feed Use*; Chesson, A., Ørskov, E. R., Eds.; Elsevier Applied Science: London, 1989; pp 25−49.

(18) Pillonel, C.; Mulder, M. M.; Boon, J. J.; Forster, B.; Binder, A. Involvement of cinnamyl-alcohol dehydrogenase in the control of lignin formation in *Sorghum bicolor* L. Moench. *Planta* **1991**, *185*, 538−544.

(19) Halpin, C.; Knight, M. E.; Foxon, G. A.; Campbell, M. M.; Boudet, A. M.; Boon, J. J.; Chabbert, B.; Tollier, M.-T.; Schuch, W. Manipulation of lignin quality by down-regulation of cinnamyl alcohol dehydrogenase. *Plant J.* **1994**, *6*, 339−350.

(20) Mulder, M. M.; Van der Hage, E. R. E.; Boon, J. J. Analytical *in source* pyrolytic methylation electron impact mass spectrometry of phenolic acids in biological matrices. *Phytochem. Anal.* **1992**, *3*, 165−172.

(21) Vermerris, W.; McIntyre, L. M. Time to flowering in *brown midrib* mutants of maize: an alternative approach to the analysis of developmental traits. *Heredity* **1999**, *83*, 171−178.

(22) Hoogerbrugge, R.; Willig, S. J.; Kistemaker, P. G. Discriminant-analysis by double stage principal component analysis. *Anal. Chem.* **1983**, *55*, 1710−1712.

(23) Klap, V. A.; Boon, J. J.; Hemminga, M. A.; Van Soelen, J. Assessment of the molecular composition of particulate organic matter exchanged between the Saeftinghe salt marsh (southwestern Netherlands) and the adjacent water system. *Marine Chem.* **1996**, *54*, 221−243.

(24) Johnson, R. A.; Wichern, D. W. *Applied Multivariate Statistical Analysis*; Prentice Hall: Englewood Cliffs, NJ, 1992.
(25) Suzuki, S.; Lam, T. B. T.; Iiyama, K. 5-Hydroxyguaiacyl nuclei as aromatic constituents of native lignin. *Phytochemistry* **1997**, *46*, 695−700.
(26) Morrison, T. A.; Kessler, J. R.; Hatfield, R. D.; Buxton, D. R. Activity of two lignin biosynthesis enzymes during development of maize internode. *J. Sci. Food. Agric.* **1994**, *65*, 113−139.
(27) Ralph, J.; MacKay, J. J.; Hatfield, R. D.; O'Malley, D. M.; Whetten, R. W.; Sederoff, R. R. Abnormal lignin in a loblolly pine mutant. *Science* **1997**, *277*, 235−238.
(28) Ralph, J.; Hatfield, R. D.; Piquemal, J.; Yahiaoui, N.; Pean, M.; Lapierre, C.; Boudet, A. M. NMR characterization of altered lignins extracted from tobacco plants down-regulated for lignification enzymes cinnamyl alcohol dehydrogenase and cinnamyl-CoA reductase. *Proc. Natl. Acad. Sci. U.S.A.* **1998**, *95*, 12803−12808.
(29) Hu, W.-J.; Harding, S. A.; Lung, J.; Popko, J. L.; Ralph, J.; Stokke, D. D.; Tsai, C.-J.; Chiang, V. L. Repression of lignin biosynthesis promotes cellulose accumulation and growth in transgenic trees. *Nature Biotech.* **1999**, *17*, 808−812.
(30) Chen, F.; Yasuda, S.; Fukushima, K. Evidence for a novel biosynthetic pathway that regulates the ratio of syringyl to guaiacyl residues in lignin in the differentiating xylem of *Magnolia kobus* DC. *Planta* **1999**, *207*, 597−603.
(31) Humphreys, J. M.; Hemm, M. R.; Chapple, C. New routes for lignin biosynthesis defined by biochemical characterization of recombinant ferulate 5-hydroxylase, a multifunctional cytochrome P450-dependent monooxygenase. *Proc. Natl. Acad. Sci. U.S.A.* **1999**, *96*, 10045−10050.
(32) Osakabe, K.; Tsao, C. C.; Li, L.; Popko, J. L.; Umezawa, T.; Carraway, D. T.; Smeltzer, R. H.; Joshi, C. P.; Chiang, V. L. Coniferyl aldehyde 5-hydroxylation and methylation direct syringyl lignin biosynthesis in angiosperms. *Proc. Natl. Acad. Sci. U.S.A.* **1999**, *96*, 8955−8960.
(33) Gang, D. R.; Costa, M. A.; Fujita, M.; Dinkova-Kostova, A. T.; Wang, H.-B.; Burlat, V.; Martin, W.; Sarkanen, S.; Davin, L. B.; Lewis, N. G. Regiochemical control of monolignol radical coupling: a new paradigm for lignin and lignan biosynthesis. *Chem. Biol.* **1999**, *6*, 143−151.
(34) McDougall, G. J.; Stewart, D.; Morrison, I. M. Tyrosine residues enhance cross-linking of synthetic proteins into lignin dehydrogenation products. *Phytochemistry* **1996**, *41*, 43−47.
(35) Domingo, C.; Saurí, A.; Mansilla, E.; Conejero, V.; Vera, P. Identification of a novel peptide motif that mediates cross-linking of proteins to cell walls. *Plant J.* **1999**, *20*, 563−570.
(36) Tamagnone, L.; Merida, A.; Parr, A.; Mackay, S.; Culianez-Macia, F. A.; Roberts, K.; Martin, C. The AmMYB308 and AmMYB330 transcription factors from Antirrhinum regulate phenylpropanoid and lignin biosynthesis in transgenic tobacco. *Plant Cell* **1998**, *10*, 135−154.
(37) Neustaedter, D. A.; Lee, S. P.; Douglas, C. J. A novel parsley *4CL1 cis*-element is required for developmentally regulated expression and protein-DNA complex formation. *Plant J.* **1999**, *18*, 77−88.

Received for review June 19, 2000. Revised manuscript received November 2, 2000. Accepted November 3, 2000. Part of this work was carried out at North Carolina State University (Raleigh, NC) with financial support for W. V. from the McKnight Foundation, a Tri-Agency (NSF−DOE−NIH) grant, and the NCSU Graduate School. The mass spectrometric work is part of the approved research program FOM28 of the Stichting FOM (Foundation for Fundamental Research of Matter) which is subsidized by The Netherlands Organisation for Scientific Research (NWO).

JF000740R